Single-spin azimuthal asymmetry in exclusive electroproduction of π^+ mesons on transversely polarized protons

A. Airapetian[l,o], N. Akopov[z], Z. Akopov[e], E.C. Aschenauer[f], W. Augustyniak[y], A. Avetissian[z], E. Avetisyan[e], B. Ball[o], S. Belostotski[r], N. Bianchi[j], H.P. Blok[q,x], H. Böttcher[f], C. Bonomo[i], A. Borissov[e], V. Bryzgalov[s], J. Burns[m], M. Capiluppi[i], G.P. Capitani[j], E. Cisbani[u], G. Ciullo[i], M. Contalbrigo[i], P.F. Dalpiaz[i], W. Deconinck[e,o], R. De Leo[b], L. De Nardo[o,e], E. De Sanctis[j], M. Diefenthaler[n,h], P. Di Nezza[j], J. Dreschler[q], M. Düren[l], M. Ehrenfried[l], G. Elbakian[z], F. Ellinghaus[d], R. Fabbri[f], A. Fantoni[j], L. Felawka[v], S. Frullani[u], D. Gabbert[f], V. Gapienko[s], F. Garibaldi[u], V. Gharibyan[z], F. Giordano[e,i], S. Gliske[o], C. Hadjidakis[j], M. Hartig[e], D. Hasch[j], G. Hill[m], A. Hillenbrand[f], M. Hoek[m], Y. Holler[e], I. Hristova[f], Y. Imazu[w], A. Ivanilov[s], H.E. Jackson[a], H.S. Jo[k], S. Joosten[n,k], R. Kaiser[m], T. Keri[m,l], E. Kinney[d], A. Kisselev[r], N. Kobayashi[w], V. Korotkov[s], P. Kravchenko[r], L. Lagamba[b], R. Lamb[n], L. Lapikás[q], I. Lehmann[m], P. Lenisa[i], L.A. Linden-Levy[n], A. López Ruiz[k], W. Lorenzon[o], X.-G. Lu[f], X.-R. Lu[w], B.-Q. Ma[c], D. Mahon[m], N.C.R. Makins[n], S.I. Manaenkov[r], L. Manfré[u], Y. Mao[c], B. Marianski[y], B. Martinez de la Ossa[d], H. Marukyan[z], C.A. Miller[v], Y. Miyachi[w], A. Movsisyan[z], V. Muccifora[j], M. Murray[m], A. Mussgiller[e,h], E. Nappi[b], Y. Naryshkin[r], A. Nass[h], W.-D. Nowak[f], L.L. Pappalardo[i], R. Perez-Benito[l], P.E. Reimer[a], A.R. Reolon[j], C. Riedl[f], K. Rith[h], G. Rosner[m], A. Rostomyan[e], J. Rubin[n], D. Ryckbosch[k], Y. Salomatin[s], F. Sanftl[t], A. Schäfer[t], G. Schnell[f,k], K.P. Schüler[e], B. Seitz[m], T.-A. Shibata[w], V. Shutov[g], M. Stancari[i], M. Statera[i], J.J.M. Steijger[q], H. Stenzel[l], J. Stewart[f], S. Taroian[z], A. Terkulov[p], A. Trzcinski[y], M. Tytgat[k], A. Vandenbroucke[k], P.B. van der Nat[q], Y. Van Haarlem[k], C. Van Hulse[k], M. Varanda[e], D. Veretennikov[r], V. Vikhrov[r], I. Vilardi[b], C. Vogel[h], S. Wang[c], S. Yaschenko[f,h], H. Ye[c], Z. Ye[e], S. Yen[v], W. Yu[l], D. Zeiler[h], B. Zihlmann[e], P. Zupranski[y]

[a] *Physics Division, Argonne National Laboratory, Argonne, Illinois 60439-4843, USA*
[b] *Istituto Nazionale di Fisica Nucleare, Sezione di Bari, 70124 Bari, Italy*
[c] *School of Physics, Peking University, Beijing 100871, China*
[d] *Nuclear Physics Laboratory, University of Colorado, Boulder, Colorado 80309-0390, USA*
[e] *DESY, 22603 Hamburg, Germany*
[f] *DESY, 15738 Zeuthen, Germany*
[g] *Joint Institute for Nuclear Research, 141980 Dubna, Russia*
[h] *Physikalisches Institut, Universität Erlangen-Nürnberg, 91058 Erlangen, Germany*
[i] *Istituto Nazionale di Fisica Nucleare, Sezione di Ferrara and Dipartimento di Fisica, Università di Ferrara, 44100 Ferrara, Italy*
[j] *Istituto Nazionale di Fisica Nucleare, Laboratori Nazionali di Frascati, 00044 Frascati, Italy*
[k] *Department of Subatomic and Radiation Physics, University of Gent, 9000 Gent, Belgium*
[l] *Physikalisches Institut, Universität Gießen, 35392 Gießen, Germany*
[m] *Department of Physics and Astronomy, University of Glasgow, Glasgow G12 8QQ, United Kingdom*
[n] *Department of Physics, University of Illinois, Urbana, Illinois 61801-3080, USA*
[o] *Randall Laboratory of Physics, University of Michigan, Ann Arbor, Michigan 48109-1040, USA*
[p] *Lebedev Physical Institute, 117924 Moscow, Russia*
[q] *National Institute for Subatomic Physics (Nikhef), 1009 DB Amsterdam, The Netherlands*
[r] *Petersburg Nuclear Physics Institute, Gatchina, Leningrad region 188300, Russia*
[s] *Institute for High Energy Physics, Protvino, Moscow region 142281, Russia*
[t] *Institut für Theoretische Physik, Universität Regensburg, 93040 Regensburg, Germany*
[u] *Istituto Nazionale di Fisica Nucleare, Sezione Roma 1, Gruppo Sanità and Physics Laboratory, Istituto Superiore di Sanità, 00161 Roma, Italy*
[v] *TRIUMF, Vancouver, British Columbia V6T 2A3, Canada*
[w] *Department of Physics, Tokyo Institute of Technology, Tokyo 152, Japan*
[x] *Department of Physics, VU University, 1081 HV Amsterdam, The Netherlands*
[y] *Andrzej Soltan Institute for Nuclear Studies, 00-689 Warsaw, Poland*
[z] *Yerevan Physics Institute, 375036 Yerevan, Armenia*

Abstract

Exclusive electroproduction of π^+ mesons was studied by scattering 27.6 GeV positrons or electrons off a transversely polarized hydrogen target. The single-spin azimuthal asymmetry with respect to target polarization was measured as a function of the Mandelstam variable t, the Bjorken scaling variable x_B, and the virtuality Q^2 of the exchanged photon. The extracted Fourier components of the asymmetry were found to be consistent with zero, except one that was found to be large and that involves interference of contributions from longitudinal and transverse virtual photons.

Key words:
PACS: 13.60.-r, 13.60.Le, 13.85.Lg, 14.20.Dh, 14.40.Aq

Generalized Parton Distributions (GPDs) [1, 2, 3] provide a three-dimensional representation of the nucleon structure at the partonic level correlating the longitudinal momentum fraction of a parton with its transverse spatial coordinates [4, 5, 6, 7, 8]. The possibility to study GPDs relies on factorization theorems proven in the framework of perturbative quantum chromodynamics for hard exclusive processes at leading twist, in particular for hard production of mesons by longitudinal virtual photons [9]. For recent theoretical reviews, see [10, 11, 12].

In the description of hard exclusive electroproduction of pseudoscalar mesons at leading twist, only the two GPDs $\widetilde{H}$ and $\widetilde{E}$ appear. Spin-averaged and spin-dependent cross sections are sensitive to different combinations of $\widetilde{H}$ and $\widetilde{E}$. It was predicted that for exclusive production of π^+ mesons on transversely polarized protons by longitudinal virtual photons the interference between the pseudovector ($\propto \widetilde{H}$) and pseudoscalar ($\propto \widetilde{E}$) contributions to the cross section leads to a large proton-spin related azimuthal asymmetry [13, 14]. Unlike the spin-averaged cross section, this asymmetry is directly proportional to the sine of the relative phase between $\widetilde{H}$ and $\widetilde{E}$. It was shown that next-to-leading order corrections in the strong-coupling constant α_s cancel in the asymmetry [15, 16]. No GPD-based model predictions are available for the production of π^+ mesons by transverse virtual photons as no factorization theorems exist for this case, but also because the leading-twist contribution is expected to be dominant. Measurements of the asymmetry are considered to be a valuable source of information about possible contributions from transverse virtual photons [17]. In a Fourier expansion of the proton-spin-dependent part of the hard exclusive pion electroproduction cross section [18] the only leading-twist contribution to the asymmetry from longitudinal virtual photons is the $\sin(\phi-\phi_S)$ Fourier amplitude, which can be used to test GPD models. All other amplitudes involve contributions from transverse virtual photons. Here, following the Trento conventions [19], ϕ and ϕ_S are the azimuthal angles in the proton rest frame of the pion-momentum and the proton-polarization vectors, respectively, measured about the virtual-photon momentum vector relative to the lepton scattering plane. For recent theoretical analyses of exclusive pion electroproduction, see [17, 20, 21].

The HERMES collaboration has previously performed measurements of the spin-averaged cross section [22] and the single-spin azimuthal asymmetry in exclusive π^+ electroproduction on longitudinally polarized protons [23]. This letter reports the first measurement of the single-spin azimuthal asymmetry for the hard exclusive reaction $ep^\uparrow \to en\pi^+$ on transversely polarized protons. The kinematic variables relevant for the analysis of this process are the squared four-momentum of the exchanged virtual photon $q^2 \equiv -Q^2$, the Bjorken variable $x_\mathrm{B} \equiv Q^2/(2M_p\nu)$, and the squared four-momentum transfer $t \equiv (q-p_{\pi^+})^2$. Here, M_p is the proton mass, ν the energy of the virtual photon in the target rest frame, and p_{π^+} the four-momentum of the pion. Instead of t, the quantity $t' \equiv t - t_0$ is used in the analysis, where $-t_0$ represents the minimum value of $-t$ for a given value of Q^2 and x_B.

The data corresponding to an integrated luminosity of $0.2\,\mathrm{fb}^{-1}$ were collected with the HERMES spectrometer [24] in the years 2002-2005. The 27.6 GeV positron or electron beam was scattered off the transversely nuclear-polarized gaseous hydrogen target internal to the HERA storage ring at DESY. The open-ended target cell was fed by an atomic-beam source [25] based on Stern-Gerlach separation combined with radiofrequency transitions of hydrogen hyperfine states. The nuclear polarization of the atoms was flipped at 1-3 minute time intervals, while both this polarization and the atomic fraction inside the target cell were continuously measured [26]. The average magnitude of the transverse polarization of the target with respect to the beam direction was $|P_\mathrm{T}| = 0.72 \pm 0.06$.

Events were selected with exactly two tracks of charged particles: a lepton and a pion. Furthermore, it was required that no additional energy deposition was detected in the electromagnetic calorimeter. The HERMES geometrical acceptance of ± 170 mrad horizontally and $\pm(40$-$140)$ mrad vertically resulted in detected scattering angles ranging from 40 mrad to 220 mrad. Leptons were identified with an average efficiency of 98% and a hadron contamination of less than 1% by using an electromagnetic calorimeter, a transition-radiation detector, a preshower scintillation counter, and a dual-radiator ring imaging Čerenkov detector [27]. Pions were identified in the momentum range $2\,\mathrm{GeV} < p < 15\,\mathrm{GeV}$ using the Čerenkov detector. For this momentum range the pion identification efficiency was on average 99% and the contamination from other hadrons less than 2%. The kinematic requirement $Q^2 > 1\,\mathrm{GeV}^2$ was imposed on the scattered lepton in order to select the hard scattering regime.

The single-spin asymmetry for exclusive π^+ production with unpolarized (U) beam and target polarization transverse (T) to the lepton (ℓ) beam direction is defined as

$$A_{\mathrm{UT},\ell}(\phi,\phi_S) = \frac{1}{|P_\mathrm{T}|}\frac{\mathrm{d}\sigma^\uparrow(\phi,\phi_S) - \mathrm{d}\sigma^\downarrow(\phi,\phi_S)}{\mathrm{d}\sigma^\uparrow(\phi,\phi_S) + \mathrm{d}\sigma^\downarrow(\phi,\phi_S)}, \quad (1)$$

where $\mathrm{d}\sigma^{\uparrow(\downarrow)}(\phi,\phi_S) = \mathrm{d}\sigma_{\mathrm{UU}}(\phi) + P_\mathrm{T}\,\mathrm{d}\sigma_{\mathrm{UT},\ell}(\phi,\phi_S)$ is a sum of the spin-averaged and spin-dependent cross sections, with $P_\mathrm{T}/|P_\mathrm{T}|$ equal to 1 (-1) for the $\uparrow$ ($\downarrow$) orientations of the transverse target polarization vector $\boldsymbol{P}_\mathrm{T}$. Both numerator and denominator of (1) can be Fourier-decomposed [18], respectively, as

$$\mathrm{d}\sigma_{\mathrm{UT},\ell}(\phi,\phi_S) \propto 2\langle\sin(\phi-\phi_S)\rangle_{\mathrm{UT},\ell}\sin(\phi-\phi_S) + \ldots, \quad (2)$$

where the ellipsis denotes five more terms omitted here for brevity, and

$$\begin{aligned}\mathrm{d}\sigma_{\mathrm{UU}}(\phi) \propto 1 &+ 2\langle\cos\phi\rangle_{\mathrm{UU}}\cos\phi \\ &+ 2\langle\cos(2\phi)\rangle_{\mathrm{UU}}\cos(2\phi).\end{aligned} \quad (3)$$

Ideally, the Fourier amplitudes in (2), which provide most direct access to the photoabsorption subprocesses, should be measured, e.g.,

$$\begin{aligned}&\langle\sin(\phi-\phi_S)\rangle_{\mathrm{UT},\ell}\\&=\frac{\int \mathrm{d}\phi\mathrm{d}\phi_S\,\sin(\phi-\phi_S)\,\mathrm{d}\sigma_{\mathrm{UT},\ell}(\phi,\phi_S)}{\int \mathrm{d}\phi\mathrm{d}\phi_S\,\mathrm{d}\sigma_{\mathrm{UU}}(\phi)}.\end{aligned}\tag{4}$$

For experimental reasons, mainly to minimize effects of the HERMES spectrometer acceptance in ϕ, the Fourier amplitudes associated with the asymmetry (1) were extracted instead, e.g.,

$$A_{\mathrm{UT},\ell}^{\sin(\phi-\phi_S)}=\frac{1}{4\pi^2}\int \mathrm{d}\phi\mathrm{d}\phi_S\,\sin(\phi-\phi_S)\,\frac{\mathrm{d}\sigma_{\mathrm{UT},\ell}(\phi,\phi_S)}{\mathrm{d}\sigma_{\mathrm{UU}}(\phi)}.\tag{5}$$

Similar equations hold for the other five amplitudes. These amplitudes embody all the essential information that could also be extracted from (2). For small (or zero) values of $\langle\cos\phi\rangle_{\mathrm{UU}}$ and $\langle\cos(2\phi)\rangle_{\mathrm{UU}}$, the amplitude in (5) corresponds to the one in (4).

The set of six Fourier amplitudes of the asymmetry was obtained from the observed π^+ event sample using a maximum likelihood fit. The distribution of events was parameterized by the probability density function $\mathcal{N}_{\mathrm{par}}$ defined as

$$\mathcal{N}_{\mathrm{par}}(P_{\mathrm{T}},\phi,\phi_S;\boldsymbol{\eta}_{\mathrm{UT},\ell})=1+P_{\mathrm{T}}\,\mathcal{A}_{\mathrm{UT},\ell}(\phi,\phi_S;\boldsymbol{\eta}_{\mathrm{UT},\ell}),\tag{6}$$

where

$$\begin{aligned}&\mathcal{A}_{\mathrm{UT},\ell}(\phi,\phi_S;\boldsymbol{\eta}_{\mathrm{UT},\ell})\\&=A_{\mathrm{UT},\ell}^{\sin(\phi-\phi_S)}\sin(\phi-\phi_S)+A_{\mathrm{UT},\ell}^{\sin(\phi+\phi_S)}\sin(\phi+\phi_S)\\&+A_{\mathrm{UT},\ell}^{\sin\phi_S}\sin\phi_S+A_{\mathrm{UT},\ell}^{\sin(2\phi-\phi_S)}\sin(2\phi-\phi_S)\\&+A_{\mathrm{UT},\ell}^{\sin(3\phi-\phi_S)}\sin(3\phi-\phi_S)+A_{\mathrm{UT},\ell}^{\sin(2\phi+\phi_S)}\sin(2\phi+\phi_S).\end{aligned}\tag{7}$$

Here, $\boldsymbol{\eta}_{\mathrm{UT},\ell}$ represents the set of six Fourier amplitudes of the sine-modulation terms in (5).

Within the maximum likelihood scheme [28], the logarithm of the likelihood function to be minimized is taken as

$$\begin{aligned}&\mathcal{L}(P_{\mathrm{T}}^i,\phi^i,\phi_S^i;\boldsymbol{\eta}_{\mathrm{UT},\ell})\\&=-\sum_{i=1}^{N_{\pi^+}}\ln[1+P_{\mathrm{T}}^i\,\mathcal{A}_{\mathrm{UT},\ell}(\phi^i,\phi_S^i;\boldsymbol{\eta}_{\mathrm{UT},\ell})],\end{aligned}\tag{8}$$

where $N_{\pi^+}=N_{\pi^+}^{\uparrow}+N_{\pi^+}^{\downarrow}$ is the total number of events in the selected data sample.

The raw results from the likelihood minimization of (8) were corrected for background contributions in order to estimate the true results for exclusive π^+ production:

$$A_{\mathrm{t}}=\frac{A_{\mathrm{r}}-b\,A_{\mathrm{b}}}{1-b}.\tag{9}$$

Here, A_{r} stands for one of the six Fourier amplitudes in $\boldsymbol{\eta}_{\mathrm{UT},\ell}$ (see (7), (8)), b and A_{b} for the fractional contribution and corresponding Fourier amplitude of the background, and A_{t} for the resulting true amplitude. The background fraction is

$$b=\frac{N_{\pi^+}-N_{\pi^+}^{\mathrm{excl}}}{N_{\pi^+}},\tag{10}$$

where $N_{\pi^+}^{\mathrm{excl}}$ is the number of exclusive events in the selected data sample.

The following analysis was performed to estimate the quantities in (9). As the recoiling neutron in the process $ep^{\uparrow}\to en\pi^+$ was not detected, the sample of "exclusive" events was selected by requiring that the squared missing mass M_X^2 of the reaction $ep^{\uparrow}\to e\pi^+X$ corresponds to the squared neutron mass M_n^2. The exclusive π^+ channel could not be completely separated from the channels with final states π^++X (defined as background channels for $X\neq n$) in which the π^+ originates, e.g., from neutral-meson (mainly ρ^0) decays, semi-inclusive processes, or nucleon resonance production, as their M_X^2 values were smeared into the region around M_n^2 due to the experimental resolution. These background events were subtracted from N_{π^+} following the method briefly outlined below, and previously employed in the analysis of the exclusive π^+ cross section [22]. Figure 1 shows the squared missing-mass dependence of the normalized yields N_{π^+} and N_{π^-} for data and a PYTHIA [29] Monte Carlo simulation. The exclusive π^+ yield was obtained by subtracting the yield difference $(N_{\pi^+}-N_{\pi^-})$ of the PYTHIA simulation from that of the data, with both differences being independently absolutely normalized (Fig. 1, middle panel):

$$N_{\pi^+}^{\mathrm{excl}}=(N_{\pi^+}-N_{\pi^-})^{\mathrm{data}}-(N_{\pi^+}-N_{\pi^-})^{\mathrm{PYTHIA}}.\tag{11}$$

The PYTHIA generator was used in conjunction with a set of JETSET [30] fragmentation parameters that had previously been adjusted to reproduce exclusive vector meson production data [31] and multiplicity distributions [32] observed by HERMES. Exclusive production of single pions is absent in PYTHIA. Note that exclusive π^- mesons cannot be produced on protons. The constraint on the invariant mass of the initial photon-nucleon system $W^2>10\,\mathrm{GeV}^2$ was applied, and the pion momentum was required to satisfy $7\,\mathrm{GeV}<p<15\,\mathrm{GeV}$. Both conditions, applied to the data and the PYTHIA yields, allowed for a better description of the data by the PYTHIA Monte Carlo simulation for values of M_X^2 outside the region corresponding to exclusive π^+ production. The resulting M_X^2 distribution of $N_{\pi^+}^{\mathrm{excl}}$ shown in the bottom panel of Fig. 1 and its resolution of $0.7\,\mathrm{GeV}^2$ were found to be almost independent of kinematic variables and consistent with that of a Monte Carlo sample of exclusive π^+ events normalized to the data (including radiative effects) [22].

An "exclusive region" in M_X^2 was defined by requiring $-1.2\,\mathrm{GeV}^2<M_X^2<1.2\,\mathrm{GeV}^2$. The lower limit corre-

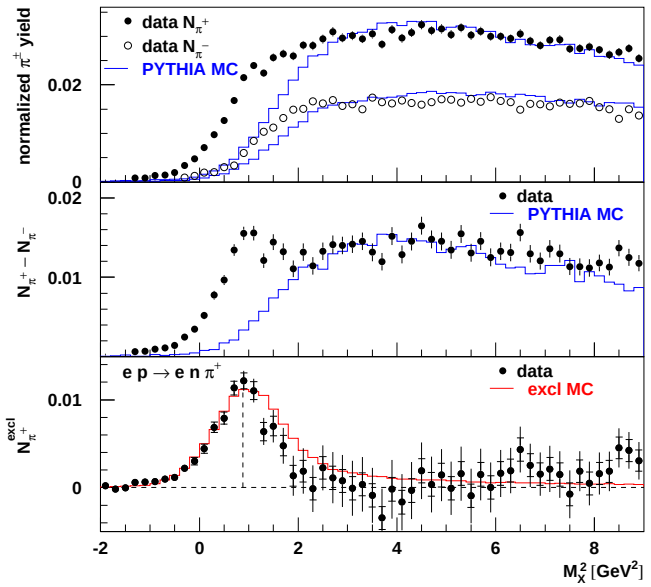

Figure 1: Upper two panels: The squared missing-mass dependence of the normalized yields $N_{\pi+}$ and $N_{\pi-}$, and of the normalized-yield difference $(N_{\pi+} - N_{\pi-})$ for data (circles) and a PYTHIA Monte Carlo simulation that does not contain exclusive production of single pions (histogram). The error bars represent the statistical uncertainty. Bottom panel: squared missing-mass dependence of the exclusive π^+ sample after background subtraction. Data (full circles) are compared to a Monte Carlo sample for exclusive π^+ production (histogram) normalized to the data. The inner error bars represent the statistical uncertainties and the outer error bars represent the quadratic sum of statistical and systematic uncertainties. The latter originate from the background subtraction procedure. The dashed vertical line indicates the squared neutron mass.

sponds to three times the resolution of M_X^2, while the upper limit was set in order to minimize the (quadratically) combined statistical and systematic uncertainties of the extracted Fourier amplitudes. The number of events $N_{\pi+}$ is 3425, while the number of events $N^{\rm excl}_{\pi^+}$ after background subtraction is 1986. A relative systematic uncertainty of 20% was assigned to $N^{\rm excl}_{\pi^+}$, which corresponds to the largest data-to-PYTHIA discrepancy outside of the exclusive region [22]. As the M_X^2 spectrum of the positron-beam data is found to be shifted by approximately 0.16 GeV^2 towards higher values relative to that of the electron-beam data, the exclusive region for the positron data is shifted accordingly. One quarter of the effect of this shift on the results presented below is assigned as a contribution to the systematic uncertainty.

The values of $A_{\rm r}$ and b in (9) are measured in the exclusive region. As the background originates from resolution smearing of events occurring at higher missing mass, $A_{\rm b}$ in (9) was assumed to be equal to the Fourier amplitude measured in the M_X^2 region between 1.9 GeV^2 and 3.3 GeV^2 where the contribution of exclusive π^+ events is negligible. In that region $A_{\rm b}$ was found to vary smoothly, with values smaller than ± 0.1, except for the $\sin\phi_S$ modulation for which it amounts on average to (0.25 ± 0.04). In order to account for a possible variation of $A_{\rm b}$ with M_X^2 in the exclusive region, one half of the difference between $A_{\rm t}$ and $A_{\rm r}$ is conservatively assigned as a contribution to the systematic uncertainty of $A_{\rm t}$.

The values of t' were calculated from the measurement of the four-momenta of the scattered lepton and produced pion by setting $M_X = M_n$, which improved the t'-resolution by a factor of two. The kinematic range that contains the events used in the subsequent analysis is defined by the following requirements on the variables: $-t' < 0.7\,{\rm GeV}^2$, $0.03 < x_{\rm B} < 0.35$, and $1\,{\rm GeV}^2 < Q^2 < 10\,{\rm GeV}^2$. The mean W^2 value of the data is 16 GeV^2.

The dominant sources of systematic uncertainty are associated with the background subtraction and correction, and the observed relative shift of the M_X^2 distributions between positron and electron data. The contributions due to the residual beam polarization of 0.02 ± 0.03, the corresponding beam-spin asymmetry [23], and the charged-track curvature in the transverse field of the target magnet, are found to be negligible. All these contributions, except for the target polarization scale uncertainty of 8.2%, are added in quadrature to yield the total systematic uncertainty. In addition, an estimate of the combined contribution to the experimental uncertainty from resolution smearing, acceptance, kinematic bin width, and effects from the detector alignment with respect to the beam is determined using a Monte Carlo simulation based on the GPD model [17] for the $\sin(\phi - \phi_S)$ Fourier amplitude only. The difference between the amplitude extracted from the Monte Carlo sample and the corresponding model prediction calculated at the average kinematic values of the Monte Carlo sample is added in quadrature to the total systematic uncertainty of $A_{{\rm UT},\ell}^{\sin(\phi-\phi_S)}$. The largest experimental uncertainties are those due to detector acceptance and kinematic bin width, and the determination of the target polarization.

Figure 2 shows the extracted Fourier amplitudes as a function of $-t'$, $x_{\rm B}$, and Q^2. For this measurement the average values of the kinematic variables are $\langle -t' \rangle = 0.18\,{\rm GeV}^2$, $\langle x_{\rm B} \rangle = 0.13$, and $\langle Q^2 \rangle = 2.38\,{\rm GeV}^2$. The background fraction b varies between $(54 \pm 6)\%$ and $(62 \pm 5)\%$ in the various kinematic bins. As $x_{\rm B}$ and $\langle Q^2 \rangle$ are correlated the average values of Q^2 vary in the four $x_{\rm B}$ bins, namely, $\langle Q^2 \rangle = 1.24,\ 1.57,\ 2.24,\ 3.91\,{\rm GeV}^2$. Analogously, the average values of x_B vary in the four Q^2 bins, $\langle x_{\rm B} \rangle = 0.07,\ 0.11,\ 0.15,\ 0.23$. A separation of the contributions from longitudinal and transverse virtual photons to the Fourier amplitudes was not possible without measurements with different beam energies. Note that in the analysis presented here there is an integration over a range in θ, with $\cos\theta \approx 1$ and $0.04 \leq \sin\theta \leq 0.15$, where θ is the angle between the beam and the virtual-photon direction.

The six Fourier amplitudes shown in Fig. 2 correspond to combinations of photoabsorption cross sections and interference terms for different photon helicities and proton-spin projections [18]. At leading twist, only $A_{{\rm UT},\ell}^{\sin(\phi-\phi_S)}$ receives a contribution from only longitudinal virtual pho-

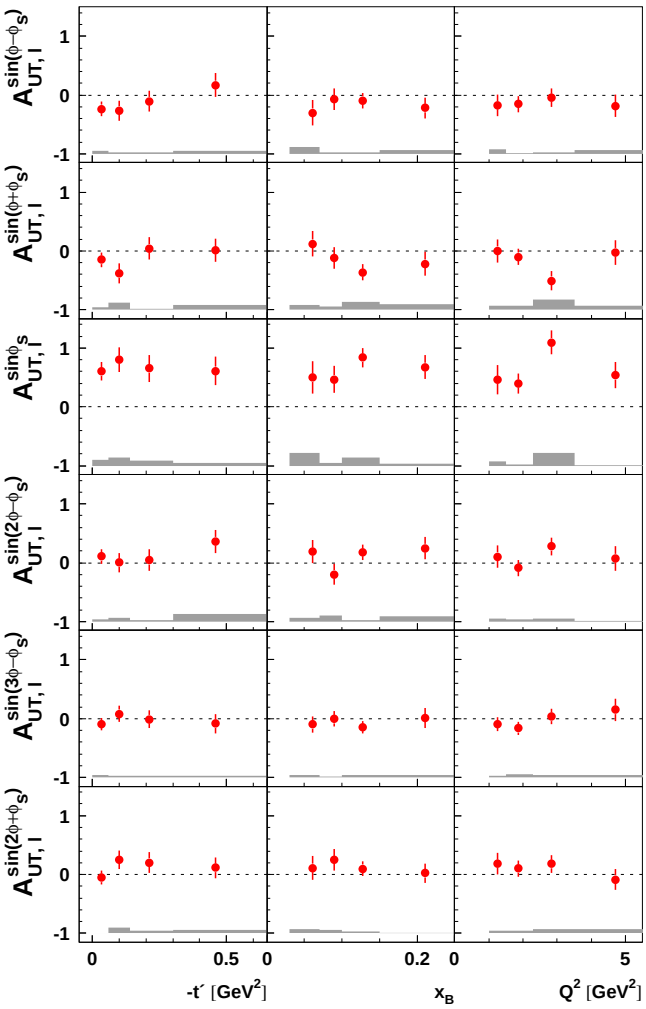

Figure 2: The set of six Fourier amplitudes ($A_{\mathrm{UT},\ell}$) describing the sine modulations of the single-spin azimuthal asymmetry for unpolarized (U) beam and transverse (T) target polarization, for the exclusive event sample. The error bars (bands) represent the statistical (systematic) uncertainties. The results receive an additional 8.2% scale uncertainty corresponding to the target polarization uncertainty.

tons, while the other Fourier amplitudes are expected to be suppressed [9] by at least one power of $1/Q$ due to interference between contributions from longitudinal and transverse virtual photons, and by $1/Q^2$ due to terms involving only transverse virtual photons.

Most of the Fourier amplitudes shown in Fig. 2 are small or consistent with zero, except $A_{\mathrm{UT},\ell}^{\sin\phi_S}$. This amplitude is found to be large and positive indicating a significant contribution from the transverse-to-longitudinal helicity transition of the virtual photon, i.e.,

$$\begin{aligned} A_{\mathrm{UT},\ell}^{\sin\phi_S} &\propto \sum_{\nu'} \mathcal{M}^*_{0\nu'++}\,\mathcal{M}_{0\nu'0-} \\ &= \mathcal{M}^*_{0+++}\,\mathcal{M}_{0+0-} + \mathcal{M}^*_{0-++}\,\mathcal{M}_{0-0-}, \end{aligned} \tag{12}$$

where $\mathcal{M}_{\mu'\nu'\mu\nu}$ are helicity amplitudes with μ' (μ) and ν' (ν) denoting the helicities of the pion (virtual photon) and the neutron (proton), respectively. These amplitudes are proportional to $\sqrt{-t'}^{|\mu-\nu-\mu'+\nu'|}$. In the framework of GPDs, the amplitude $\mathcal{M}_{0-++}$ is associated at leading twist with virtual-photon helicity flip in the t-channel [18], which is proportional to $\sqrt{-t'}$ and hence is expected to vanish for $-t' \to 0$. Among higher-twist contributions the one that involves the parton-helicity-flip GPDs H_T and $\widetilde{H}_T$ need not vanish at small values of $|t'|$. Moreover, in the more general framework of helicity amplitudes and the Regge model, $A_{\mathrm{UT},\ell}^{\sin\phi_S}$ receives contributions from natural and unnatural-parity exchange [33, 17], which allow it to remain constant as a function of $-t'$, as the data in Fig. 2 suggest. Lack of parameterizations of the photoabsorption cross sections and interference terms [18] involving transverse virtual photons does not allow further interpretation of the corresponding Fourier amplitudes. Any model that describes exclusive pion production will need to describe not only the leading-twist Fourier amplitude, but also the other contributions to the target-spin azimuthal asymmetry.

Of special interest in the present measurement is the Fourier amplitude $A_{\mathrm{UT},\ell}^{\sin(\phi-\phi_S)}$ in case of production by longitudinal photons, which can be compared with GPD models. It is related to the parton-helicity-conserving part of the scattering process and is sensitive to the interference between $\widetilde{\mathcal{H}}$ and $\widetilde{\mathcal{E}}$ [13, 16]:

$$\begin{aligned} A_{\mathrm{UT},\ell}^{\sin(\phi-\phi_S)} &= -\frac{\sqrt{-t'}}{M_p} \\ &\quad\times \frac{\xi\sqrt{1-\xi^2}\,\mathrm{Im}(\widetilde{\mathcal{E}}^*\widetilde{\mathcal{H}})}{(1-\xi^2)\widetilde{\mathcal{H}}^2 - \frac{t\xi^2}{4M_p^2}\widetilde{\mathcal{E}}^2 - 2\xi^2\,\mathrm{Re}(\widetilde{\mathcal{E}}^*\widetilde{\mathcal{H}})}, \end{aligned} \tag{13}$$

where the transition form factors $\widetilde{\mathcal{H}}$ and $\widetilde{\mathcal{E}}$ denote convolutions of hard scattering kernels and the pion distribution amplitude with the GPDs $\widetilde{H}$ and $\widetilde{E}$, respectively. Note that in the models described below terms proportional to the $\cos\phi$ and $\cos(2\phi)$ modulation of the spin-averaged cross section are not included. In the measurement presented here these terms are not known, although they nonetheless contribute to the values of the extracted Fourier amplitudes.

Figure 3 shows in more detail the extracted Fourier amplitude $A_{\mathrm{UT},\ell}^{\sin(\phi-\phi_S)}$ as a function of $-t'$. The solid and dotted curves represent the leading-twist, leading-order in α_s calculations of this amplitude for longitudinal virtual photons using two variants of the GPD model of [20]. The modelling of the GPD $\widetilde{E}$ relies here, even at larger values of $-t$, on the dominance of the pion pole $1/(m_\pi^2 - t)$ in the pion exchange amplitude, with m_π the pion mass. Then $\widetilde{\mathcal{E}}$ is real and positive, and the value of $A_{\mathrm{UT},\ell}^{\sin(\phi-\phi_S)}$ is typically predicted to be large and negative, while it must sharply vanish at the kinematic boundary $-t' = 0$ (see solid curve). The data qualitatively disagree with such a simplified GPD model. The "Regge-ized" variant of the GPD-$\widetilde{E}$ model [20], containing more than only a pion t-channel exchange, results in the dash-dotted curve. In such a model the asymmetry can become positive at

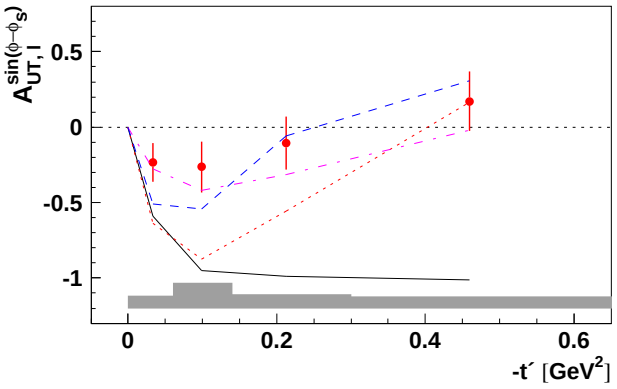

Figure 3: Model predictions for the $\sin(\phi - \phi_S)$ Fourier amplitude as a function of $-t'$. The curves represents predictions of GPD-model calculations. The full circles show the values of $A_{\mathrm{UT},\ell}^{\sin(\phi-\phi_S)}$ taken from Fig. 2. The error bars (bands) represent the statistical (systematic) uncertainties. See text for details.

larger values of $-t'$, caused by a negative real part in $\widetilde{\mathcal{E}}$. The dash-dotted curve arises from an alternative GPD approach [34], in which the imaginary part of $\widetilde{\mathcal{H}}$ becomes negative while the real part of $\widetilde{\mathcal{E}}$ remains positive at larger values of $-t'$.

An attempt to evaluate the complete set of Fourier amplitudes (7), and in particular the value of $A_{\mathrm{UT},\ell}^{\sin(\phi-\phi_S)}$, is presented in [17]. In this model, the GPDs are calculated in a similar way as in the models [15, 35], except that the experimental value of the pion form factor F_π is used. Here a large non-pole contribution from $\widetilde{E}$ over-compensates the pion-pole contribution leading to the zero-crossing behavior of the amplitude as a function of $-t'$ (see dashed curve in Fig. 3). This model appears to be qualitatively in agreement with the data. However, within the large experimental uncertainty $A_{\mathrm{UT},\ell}^{\sin(\phi-\phi_S)}$ is also consistent with zero. A vanishing Fourier amplitude in this model implies the dominance (due to the pion pole) of $\widetilde{E}$ over $\widetilde{H}$ at low $-t'$. This is in agreement with the recent HERMES measurement of the exclusive π^+ cross section [22], which is well described at $-t' = 0.1\,\mathrm{GeV}^2$ by a GPD model [35] based only on $\widetilde{E}$ while neglecting the contribution of $\widetilde{H}$.

In summary, the Fourier amplitudes of the single-spin azimuthal asymmetry are measured in exclusive electroproduction of π^+ mesons on transversely polarized protons, for the first time. Within the experimental uncertainties the amplitude of the $\sin(\phi - \phi_S)$ modulation is found to be consistent with zero, thus excluding a pure pion-pole contribution to the GPD $\widetilde{E}$ in leading-twist calculations. This could also be an indication for the dominance of $\widetilde{E}$ over the GPD $\widetilde{H}$ at low $-t'$. The observed amplitude of the $\sin\phi_S$ modulation is large and positive which implies the presence of a sizeable interference between contributions from longitudinal and transverse virtual photons. A next-to-leading twist calculation as well as knowledge of the contributions from transverse photons and their interference with longitudinal photons are required for a description of the measurements.

We gratefully acknowledge the DESY management for its support and the staff at DESY and the collaborating institutions for their significant effort. This work was supported by the FWO-Flanders and IWT, Belgium; the Natural Sciences and Engineering Research Council of Canada; the National Natural Science Foundation of China; the Alexander von Humboldt Stiftung; the German Bundesministerium für Bildung und Forschung (BMBF); the Deutsche Forschungsgemeinschaft (DFG); the Italian Istituto Nazionale di Fisica Nucleare (INFN); the MEXT, JSPS, and G-COE of Japan; the Dutch Foundation for Fundamenteel Onderzoek der Materie (FOM); the U.K. Engineering and Physical Sciences Research Council, the Science and Technology Facilities Council, and the Scottish Universities Physics Alliance; the U.S. Department of Energy (DOE) and the National Science Foundation (NSF); the Russian Academy of Science and the Russian Federal Agency for Science and Innovations; the Ministry of Economy and the Ministry of Education and Science of Armenia; and the European Community-Research Infrastructure Activity under the FP6 "Structuring the European Research Area" program (HadronPhysics, contract number RII3-CT-2004-506078).

References

[1] D. Müller, D. Robaschik, B. Geyer, F.M. Dittes, and J. Horejsi, Fortschr. Phys. 42 (1994) 101.
[2] A.V. Radyushkin, Phys. Lett. B 380 (1996) 417.
[3] X. Ji, Phys. Rev. Lett. 78 (1997) 610.
[4] M. Burkardt, Phys. Rev. D 62 (2000) 071503; Erratum–ibid. D 66 (2002) 119903.
[5] M. Diehl, Eur. Phys. J. C 25 (2002) 223; Erratum-ibid. C31 (2003) 277.
[6] J.P. Ralston and B. Pire, Phys. Rev. D 66 (2002) 111501.
[7] A.V. Belitsky and D. Müller, Nucl. Phys. A 711 (2002) 118.
[8] M. Burkardt, Int. J. Mod. Phys. A 18 (2003) 173.
[9] J.C. Collins, L.L. Frankfurt, and M. Strikman, Phys. Rev. D 56 (1997) 2982.
[10] K. Goeke, M.V. Polyakov, and M. Vanderhaeghen, Prog. Part. Nucl. Phys. 47 (2001) 401.
[11] M. Diehl, Phys. Rept. 388 (2003) 41.
[12] A.V. Belitsky and A.V. Radyushkin, Phys. Rept. 418 (2005) 1.
[13] L.L. Frankfurt, P.V. Pobylitsa, M.V. Polyakov, and M. Strikman, Phys. Rev. D 60 (1999) 014010.
[14] L.L. Frankfurt, M.V. Polyakov, M. Strikman, and M. Vanderhaeghen, Phys. Rev. Lett. 84 (2000) 2589.
[15] A.V. Belitsky and D. Müller, Phys. Lett. B 513 (2001) 349.
[16] M. Diehl and W. Kugler, Eur. Phys. J. C 52 (2007) 933.
[17] S. Goloskokov and P. Kroll, arXiv:0906.0460 [hep-ph].
[18] M. Diehl and S. Sapeta, Eur. Phys. J. C 41 (2005) 515.
[19] A. Bacchetta, U. D'Alesio, M. Diehl, and C.A. Miller, Phys. Rev. D 70 (2004) 117504.
[20] Ch. Bechler and D. Müller, arXiv:0906.2571 [hep-ph].
[21] M.M. Kraskulov and U. Mosel, arXiv:0904.4442 [hep-ph].
[22] A. Airapetian et al., Phys. Lett. B 659 (2008) 486.
[23] A. Airapetian et al., Phys. Lett. B 535 (2002) 85.
[24] K. Ackerstaff et al., Nucl. Instrum. Methods A417 (1998) 230.
[25] A. Nass et al., Nucl. Instrum. Methods A505 (2003) 633.
[26] A. Airapetian et al., Nucl. Instrum. Methods A540 (2005) 68.
[27] N. Akopov et al., Nucl. Instrum. Methods A479 (2002) 511.
[28] R. Barlow, Nucl. Instrum. Methods A297 (1990) 496.

[29] T. Sjöstrand, L. Lonnblad, and S. Mrenna, Comput. Phys. Commun. 135 (2001) 238.
[30] T. Sjöstrand, Comput. Phys. Commun. 82 (1994) 74.
[31] P. Liebing, DESY-THESIS-2004-036.
[32] A. Hillenbrand and M. Hartig for the HERMES collaboration, Proceedings of 40th Rencontres de Moriond on QCD and High Energy Hadronic Interactions, La Thuile, Aosta Valley, Italy, 12-19 Mar 2005; hep-ex/0505086.
[33] M. Diehl, *private communication*, 2008.
[34] K. Kumericki, D. Müller, and K. Passek-Kumericki, Eur. Phys. J. C 58 (2008) 193.
[35] M. Vanderhaegen, P.A.M Guichon, and M. Guidal, Phys. Rev. D 60 (1999) 094017.